ELSEVIER

Spectrochimica Acta Part B 52 (1997) 765–777

SPECTROCHIMICA ACTA PART B

Calculation of crater profiles on a flat cathode in a direct current glow discharge

A. Bogaerts*, R. Gijbels

University of Antwerp, Department of Chemistry, Universiteitsplein 1, B-2610 Wilrijk-Antwerp, Belgium

Received 23 August 1996; accepted 28 October 1996

Abstract

A three-dimensional hybrid set of models (Monte Carlo and fluid models) for the different plasma species in a glow discharge is used to calculate crater profiles on a flat cathode in the VG9000 direct current glow discharge cell. The characteristic crater profiles found experimentally are at least qualitatively predicted by the modeling work: (i) the crater is deeper at the edges than in the center (called the "crater edge effect"), (ii) the crater walls are not completely steep, (iii) the crater bottom can be concave, convex or flat, and (iv) there is a rim outside the crater profile due to redeposition of material. The crater edge effect is the most pronounced feature in the calculated profiles, and arises from the anodic front plate at 0.5 mm from the cathode surface. As this effect impairs depth resolution in depth-profiling, some modifications to the cell geometry are proposed, which are expected to eliminate or minimize this effect. © 1997 Elsevier Science B.V.

Keywords: Crater profile; Direct current glow discharge; Monte Carlo modeling

1. Introduction

Glow discharges find applications in the microelectronics industry for etching and deposition purposes [1], and as spectroscopic sources in analytical chemistry [2]. In the latter case, the material to be analyzed is used as the cathode of the glow discharge cell. Energetic plasma particles impinge on the cathode and thereby release atoms from the cathode surface (sputtering). The sputtered cathode atoms enter the glow discharge plasma, where they are subject to a variety of collisions (especially ionization and excitation). Owing to these sputtering and collision processes, the plasma is filled with atoms, ions and photons representative of the material to be analyzed. This makes the glow discharge useful as a source for a number of analytical techniques: mass spectrometry (GDMS), and atomic emission, absorption and fluorescence spectrometry (GD-AES, GD-AAS and GD-AFS). These techniques are particularly useful for the bulk analysis of metals. However, the concept of sputtering implies that the cathode is being eroded "layer after layer", and it is possible to perform elemental analysis of successive layers as a function of depth, i.e., depth-profiling. Numerous applications of depth-profiling are found in GD-AES [3–7] and, to a lesser extent, in GDMS [8–11].

For good depth-profiling practice, it is important to obtain flat crater bottoms. In practice, curved crater bottoms are often found, i.e., the erosion rate at the edges of the crater is different from that at the center. As a result, sample atoms originating from different depths enter the plasma simultaneously and the depth resolution of the analysis is reduced. The shape of

* Corresponding author.

PII S0584-8547(96)01623-0

the crater profile is strongly influenced by the discharge conditions [4,8,9]. Only at specific discharge conditions can flat crater bottoms be obtained. Stumpe et al. have presented an explanation for the occurrence of non-flat crater bottoms in sputtered neutrals mass spectrometry (SNMS), based on a concave or convex equipotential curve of the plasma [12]. Jakubowski has adopted a similar explanation for GDMS, based on the equipotential surfaces in the plasma [9,13]. The entire potential applied to the discharge falls off in the small region in front of the cathode called the cathode dark space (CDS). When the equipotential surfaces are parallel to the cathode surface, discharge gas ions bombard the cathode equally at all radial positions, and a flat crater bottom is obtained. However, when the equipotential surfaces are bent with respect to the sample surface, focussing of the bombarding ions on certain positions of the sample surface can occur, resulting in a non-flat crater bottom. This explanation has been visualized by SIMION simulations [9,13]. SIMION allows one to calculate equipotential surfaces and ion trajectories in a vacuum environment between two electrodes with different potentials [14]. In order to simulate the bombardment of ions onto the cathode surface, Jakubowski and coworkers considered the interface between the CDS and the negative glow (NG) as an electrode, and its position as a function of radial position had to be assumed, from which the equipotential surfaces were calculated. Given the equipotential surfaces, the ion trajectories were simulated, i.e., the ions were assumed to move perpendicular to these surfaces towards the cathode without any collisions (since SIMION works in a vacuum environment).

We have developed a set of three-dimensional models in which the behavior of different plasma species is described explicitly, and in which the position of the interface between CDS and NG, and the equipotential surfaces in front of the cathode, can be calculated exactly [15,16]. The trajectories of charged particles in this electric field are calculated explicitly in three dimensions, and directional changes due to collisions are taken into account. In the present paper, these models will be applied to calculate crater profiles at the cathode. These calculated profiles will be compared with experimental observations to test the validity of the model. Once we understand better the factors that are responsible for the shape of the crater profile, we can predict how to proceed to obtain good crater profiles.

2. Description of the models

A three-dimensional hybrid modeling set has been developed, consisting of different submodels for the different plasma species. The species assumed to be present in the plasma include the argon gas atoms at rest, uniformly distributed throughout the discharge, singly charged argon ions, fast argon atoms, metastable argon atoms, electrons (fast and slow groups), and sputtered analyte atoms and the corresponding ions (copper was taken as an example). These species are described with Monte Carlo and fluid models.

The fast electrons are treated with a Monte Carlo model [15,17,18]; collision processes incorporated are elastic collisions with argon atoms, electron impact excitation and ionization from the argon ground state and from the metastable level, and ionization of sputtered copper atoms. The behavior of the slow electrons and the argon ions is calculated in a fluid model [15,18]; the continuity and transport equations are coupled with the Poisson equation to obtain a self-consistent electric field distribution. Moreover, the argon ions are described with a Monte Carlo model in the cathode dark space (CDS), as are the fast argon atoms which are created by symmetric charge transfer and elastic collisions from the argon ions [15,17,19]. The collision processes taken into account are symmetric charge transfer for the argon ions, elastic collisions with argon atoms for both argon ions and fast atoms, and fast argon ion and atom impact ionization and excitation of argon atoms. The metastable argon atoms are handled with a fluid model, consisting of a balance equation with different production and loss processes [16,20]. The sputtered copper atoms and copper ions are described with a combination of Monte Carlo and fluid models. The copper atoms are sputtered away from the cathode due to the bombardment of argon ions, fast argon atoms and copper ions (see below). The flux of sputtered atoms is calculated from the flux energy distributions of the argon ions, fast argon atoms and copper ions at the cathode ($f_{Ar^+}(0,E)$, $f_{Ar^0}(0,E)$, $f_{Cu^+}(0,E)$, respectively), and an empirical formula for the sputtering yield (i.e., the number of sputtered atoms per incident particle),

adopted from ref. [21]

$$J_0 = -\int \{Y_{Ar-Cu}(E)[f_{Ar^+}(0,E)+f_{Ar^0}(0,E)] + Y_{Cu-Cu}(E)f_{Cu^+}(0,E)\}dE$$

where $Y_{Ar-Cu}(E)$ and $Y_{Cu-Cu}(E)$ present the sputtering yields of bombarding argon atoms and ions, and copper ions, respectively, on a copper cathode as a function of the bombarding particles' energies. The sputtering yield is a complex function of the incident energy and the masses and atomic numbers of the bombarding particles and the surface target. The (−)-sign indicates that the flux of sputtered copper atoms is in the opposite direction to the fluxes of the bombarding particles. The sputtered copper atoms arrive in the plasma and lose their initial energies of 5–10 eV almost immediately by collisions with the argon gas atoms until they are thermalized. This thermalization process is described with a Monte Carlo model [16,22]. The further transport of the copper atoms (diffusion dominated), the creation of copper ions (by electron impact ionization, Penning ionization by metastable argon atoms, and asymmetric charge transfer by argon ions), and the transport of these copper ions (migration and diffusion controlled), are handled in a fluid model [16,23]. Finally, the behavior of the copper ions in the CDS is also treated with a Monte Carlo model [16,23].

All these models are combined into a comprehensive modeling network, and solved iteratively until final convergence is reached, to obtain an overall picture of the glow discharge. The Monte Carlo models are developed in three dimensions and the fluid models in two dimensions (as the three dimensions can be reduced to two dimensions owing to the cylindrical symmetry of the cell), and applied to the standard cell for analyzing flat samples in the VG9000 glow discharge mass spectrometer (VG Elemental, Fisons; see Fig. 1). More information about these models can be found in refs. [15–20,22–25].

From the flux energy distributions of the plasma species bombarding the cathode (i.e., argon ions, fast argon atoms and copper ions) as a function of the radial position, obtained from the Monte Carlo models of the argon ions and fast atoms and of the copper ions, the crater profile at the cathode surface due to sputtering can be calculated. Since entire flux energy distributions at each different radial position required too much computer space, we used the fluxes and *mean energies* of the bombarding species as a function of radial position. From these fluxes and mean energies, the flux of sputtered copper atoms as a function of radial position was obtained. These "sputter fluxes" as a function of radial position were used only as relative values. The absolute values at each radial position are obtained by relating the relative numbers to the total sputter flux calculated from the total flux energy distribution at the cathode, which is more accurate.

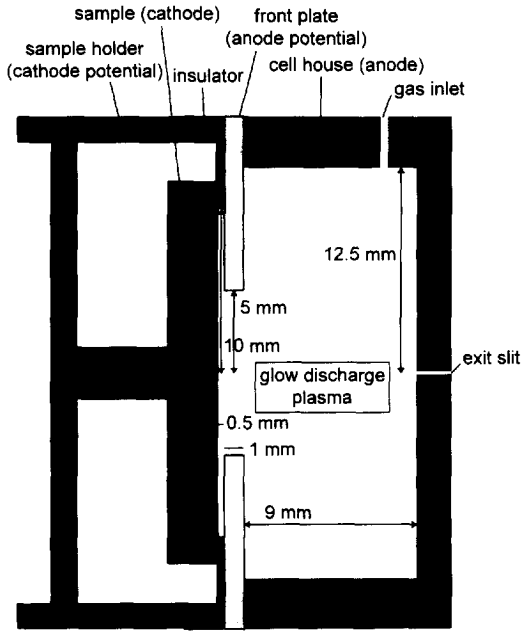

Fig. 1. Schematic representation of the VG9000 glow discharge cell geometry to which the modeling work is applied.

A considerable fraction of the sputtered atoms is, however, redeposited on the cathode due to back-diffusion. Indeed, under the present discharge conditions, the total flux of sputtered copper atoms was calculated to be 3.8×10^{16} s^{-1}, whereas the total flux of redeposited copper atoms was 2.2×10^{16} s^{-1}, leading to a net flux of sputtered atoms of 1.6×10^{16} s^{-1} (i.e., about 43% of the total sputtered flux). It is the net flux of sputtered copper atoms as a function of radial position that gives rise to the crater profile. The conversion from flux to erosion rate is accomplished in the following way [26]

$$ER = J_{\text{sput, net}} \frac{M}{N_A \rho}$$

where ER is the erosion rate (in cm s^{-1}), $J_{sput,net}$ is the net sputtered flux (in cm^{-2} s^{-1}), M and ρ are the atomic weight (g mol^{-1}) and density of the sample material (ρ_{Cu} = 8.92 g cm^{-3} [27]), and N_A is Avogadro's number. From the erosion rate as a function of radial position, the crater profile after sputtering during a certain time period is obtained.

3. Results and discussion

Fig. 2(a–c) present the total flux energy distributions of the plasma species bombarding the cathode, i.e., the argon ions, fast argon atoms and copper ions, respectively, at 1000 V, 75 Pa and 3 mA. The argon ion flux energy distribution (Fig. 2(a)) is characterized by a decreasing curve towards high energies. Indeed, the argon ions gain energy from the electric field in front of the cathode, but they also lose their energy efficiently by collisions. The fast argon atom flux energy distribution also decreases towards high energies, as can be seen in Fig. 2(b). The energy distribution drops more rapidly; because the fast argon atoms cannot gain energy from the electric field, they can only lose energy by collisions. It should be noted that the x-axis of Fig. 2(b) is truncated at 200 eV, since the part of the flux energy distribution beyond 200 eV is negligible. The flux energy distribution of the copper ions bombarding the cathode (Fig. 2(c)), on the other hand, is characterized by a pronounced peak at maximum energy. This indicates that the copper ions do not efficiently lose the energy they gained from the electric field on their way to the cathode. Comparison of the absolute values of the flux energy distributions in the three figures shows that the cathode is predominantly bombarded by fast argon atoms. The fast argon atoms are thus mainly responsible for the cathode sputtering. Their contribution was calculated to be about 73% at 1000 V, 75 Pa and 3 mA. The argon ions were found to be the second most important, with a contribution of about 26% under the present discharge conditions. Since sputtering increases with the energy of the bombarding particles, the contribution of the copper ions (i.e. self-sputtering) is not negligible, and was calculated to be $\approx$ 1%.

In Fig. 3(a–c) the fluxes of the three bombarding species at the cathode are illustrated, as a function of radial position from the cell axis, at 1000 V, 75 Pa and

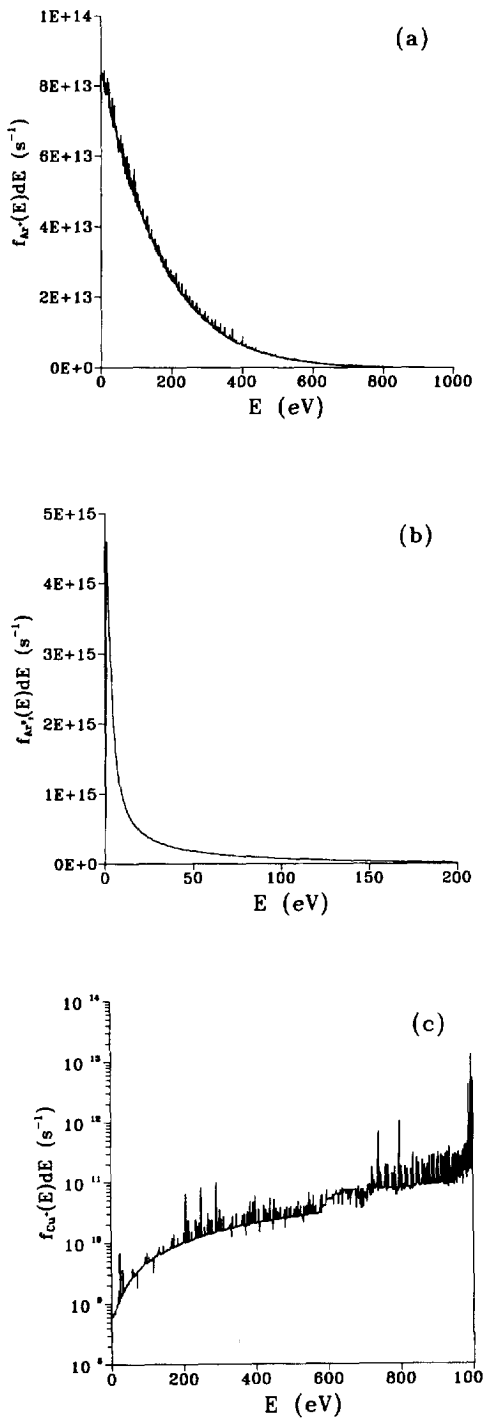

Fig. 2. Calculated flux energy distributions of (a) the argon ions; (b) fast argon atoms; and (c) copper ions, at the cathode (at 1000 V, 75 Pa, 3 mA, copper cathode in argon).

3 mA. The fluxes reach a weak maximum at 0.3–0.4 cm from the cell axis. This follows from the calculated equipotential surfaces in front of the cathode (see Fig. 4). Indeed, the equipotential surfaces are not completely parallel to the sample surface, but are bent in such a way that the plasma species are slightly focussed and bombard the cathode more at 0.3–0.4 cm from the cell axis. This corresponds to

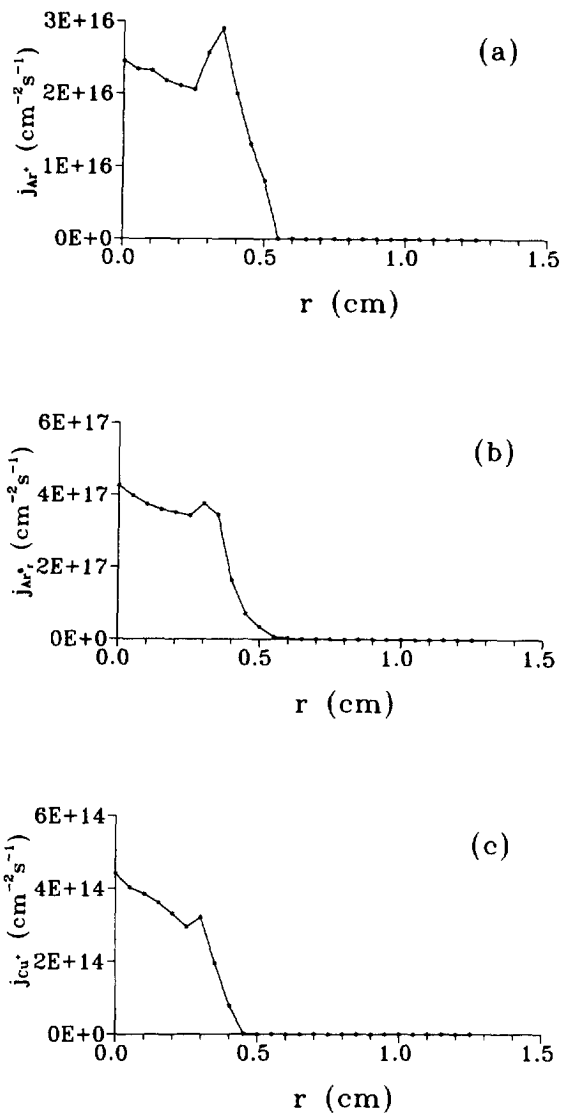

Fig. 3. Calculated fluxes of (a) the argon ions; (b) fast argon atoms; and (c) copper ions, at the cathode, as a function of radial position from the cell axis (at 1000 V, 75 Pa, 3 mA, copper cathode in argon).

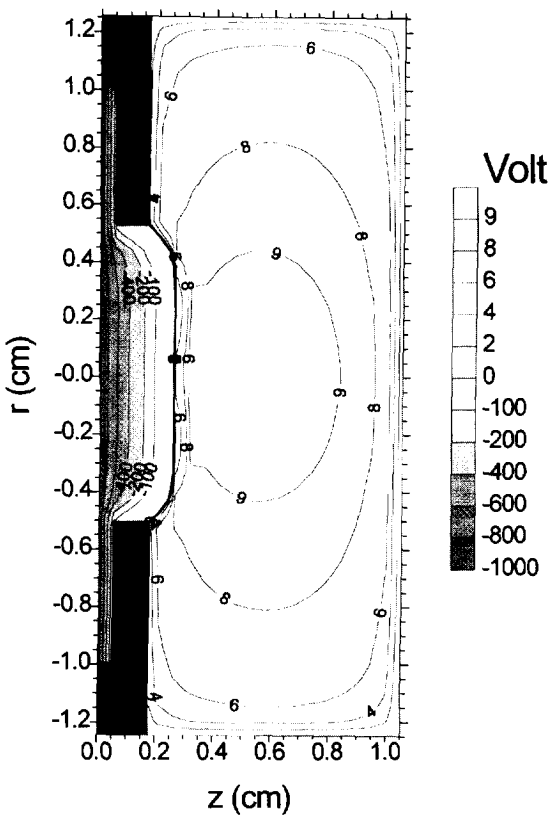

Fig. 4. Calculated electric potential distribution throughout the discharge (at 1000 V, 75 Pa, 3 mA, copper cathode in argon).

the explanation by Jakubowski using SIMION simulations [9,13], when similar equipotential surfaces are assumed as calculated in our model. The effect is most pronounced for the argon ions, since they are most clearly directed by the equipotential surfaces (i.e. they are not so much scattered in random directions by collisions; their dominant collisions are symmetric charge transfer collisions, after which they start again from rest in a direction parallel to the local electric field). The fluxes of the plasma species at the cathode are almost zero further than 0.5 cm from the cell axis. Indeed, as can be seen in Fig. 1, the cell has a front plate at 0.5 mm from the cathode with an aperture of 0.5 cm radius. Hence, only plasma species that approach the cathode within 0.5 cm from the cell axis can really impinge on the cathode.

Not only are the fluxes of the plasma species which bombard the cathode radially heterogeneous, their

mean energies at the cathode are not constant either as a function of the radial distance from the cell axis. In Fig. 5(a–c), it can be seen that the mean energies of the plasma species bombarding the cathode are at their maximum at about 0.3–0.5 cm from the cell axis. This is the result of the high electric field strengths in the vicinity of the front plate (see Fig. 6(a) and (b) in ref. [15]), which follow from the large potential drop over a small distance near the front plate, as appears from Fig. 4 (i.e., the front plate is at anode potential; hence, a potential of 1000 V has to decline over a distance of only 0.5 mm).

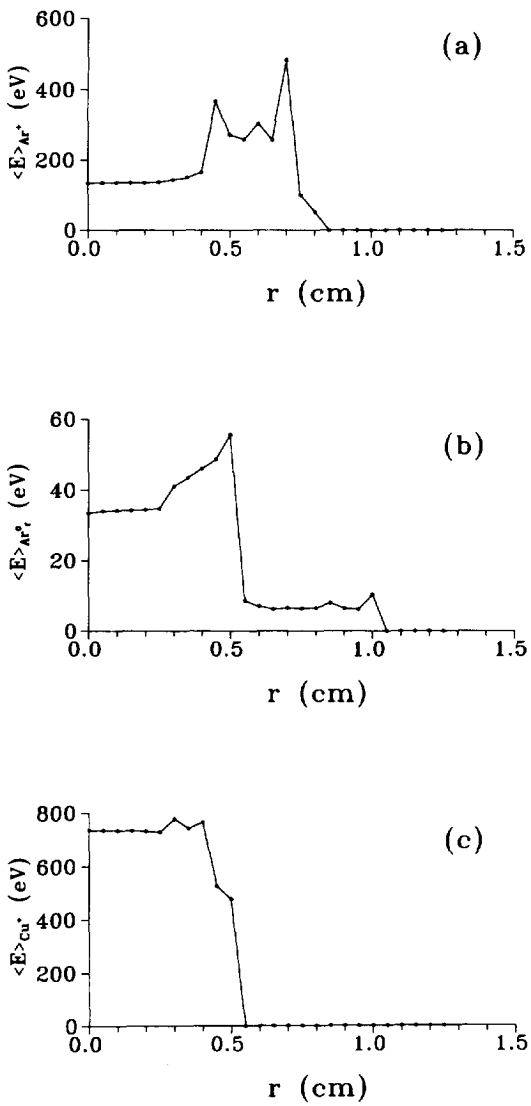

Fig. 5. Calculated mean energies of (a) the argon ions; (b) fast argon atoms; and (c) copper ions, at the cathode, as a function of radial position from the cell axis (at 1000 V, 75 Pa, 3 mA, copper cathode in argon).

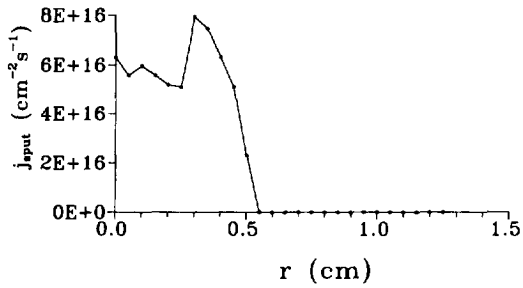

Fig. 6. Calculated flux of sputtered copper atoms from the cathode as a function of radial position from the cell axis (at 1000 V, 75 Pa, 3 mA, copper cathode in argon).

As sputtering increases both with the fluxes of the bombarding plasma species and with their energies, it follows that the amount of sputtering is the highest at about 0.3–0.5 cm from the cell axis (see Fig. 6). As stated above, a large fraction of the sputtered atoms diffuses back towards the cathode and is redeposited on the cathode surface. The flux of back-diffusing sputtered atoms on the cathode as a function of radial position is presented in Fig. 7 for 1000 V, 75 Pa and 3 mA. This flux, again, is not radially homogeneous: it is at its maximum at the cell axis, decreases only slightly to about 0.3 cm and then falls very rapidly to about 0.6 cm from the cell axis. It is interesting to note that the flux of back-diffusing atoms is not zero beyond $r = 0.5$ cm. Hence, despite the fact that there is virtually no more sputtering at 0.6 cm from the cell axis (i.e. behind the front plate; see Fig. 6), the sputtered atoms can diffuse in the radial direction to

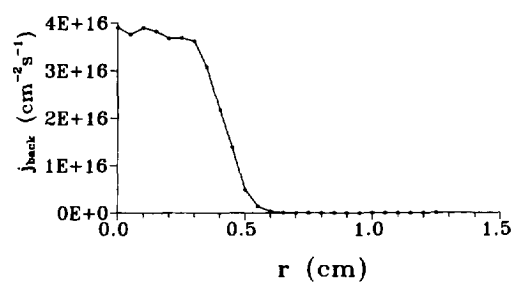

Fig. 7. Calculated flux of back-diffusing copper atoms to the cathode as a function of radial position from the cell axis (at 1000 V, 75 Pa, 3 mA, copper cathode in argon).

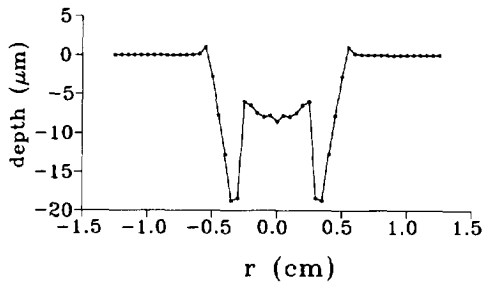

Fig. 8. Calculated crater profile on the cathode surface after sputtering for 1 h (at 1000 V, 75 Pa, 3 mA, copper cathode in argon).

positions behind the front plate, from where they can be redeposited again on the cathode. Hence, this results in a small amount of "negative sputtering" (i.e. more redeposition than sputtering) at positions further than 0.5 cm from the cell axis.

The combination of sputtering flux from the cathode and backdiffusion flux towards the cathode gives rise to the net sputtering flux at the cathode surface, from which the erosion rate and hence the crater profile after some period of sputtering can be computed. The calculated crater profile after sputtering for 1 h, at 1000 V, 75 Pa and 3 mA (and mirrored with respect to the cell axis), is presented in Fig. 8. The shape of the crater profile and the absolute values for the crater depth (order of μm) are in reasonable agreement with experiment (see for example Figs 11 and 12 below, adopted from Ref. [8]). The modeled crater is much deeper at the sides than in the center. The reason for this is explained above: (i) the equipotential surfaces in front of the cathode are not completely parallel to the sample surface, but are bent in such a way that the plasma species will bombard the cathode much more at the edges of the crater, and (ii) the energies of the bombarding plasma species are also highest at the edges of the sample surface, owing to the strong electric field in the vicinity of the front plate. The higher bombarding fluxes and the higher energies of the bombarding particles both give rise to increased sputtering and therefore to a crater which is deeper at the edges. The so-called crater edge effect [i.e. $(ER_{edge} - ER_{center})/ER_{center}$] was calculated theoretically to be about 130%. Experimentally, values ranging from 50 to 400% (and typically about 200%) are encountered for the same VG9000 glow discharge cell [8].

A second interesting feature of Fig. 8 concerns the crater bottom, which is not completely flat but more or less concave. Experimentally, concave, convex and flat crater bottoms can be obtained, depending on the discharge conditions (see below). A convex or concave crater bottom is also the result of radially inhomogeneous sputtering. Indeed, in a model where radially homogeneous sputtering was assumed [26], only a convex crater bottom could be predicted, based on radially heterogeneous redeposition. Also, the non—steep crater walls of the calculated profile, resulting from the radially heterogeneous sputtering, are backed up by the measured profiles (see below), although the effect is generally not so pronounced in the experimental results. Finally, a rim is observed in the calculated crater profile, further than 0.5 cm from the center, owing to the fact that more material is redeposited on the cathode than is sputtered away (see above). In the experimental crater profiles, such a rim is also observed, but it is more pronounced than in the calculated result (see below). Nevertheless, the modeling calculations are already able to explain at least qualitatively the typical features of experimental crater profiles.

The crater profile calculated for the present discharge conditions is not very suitable for state-of-the-art depth-profiling, because the crater bottom is not flat. We studied the influence of pressure and voltage on the calculated crater profiles, to investigate what discharge conditions would produce a more useful crater (i.e. with a flat bottom). Fig. 9 illustrates the effect of the voltage on the crater profiles after 1 h of sputtering at constant pressure. It is seen that, at increasing voltages (and currents), the depth of the crater profile increases. Indeed, when voltage and current are higher, there will be a larger flux of bombarding gas particles on the cathode, and, in addition, their energy will be higher, resulting in more sputtering. Moreover, the shapes of the crater profiles also change considerably. At low voltage and current, the calculated crater profile has a pronounced concave shape. The crater profile calculated for 600 V, 100 Pa and 1.97 mA is unfavorable for depth profiling, since the depth is not constant as a function of radial position. However, as the voltage increases (and hence also the current when pressure is kept constant) the crater bottom becomes gradually flatter, as can be observed in the crater profiles obtained for 1000, 1200 and 1400 V. The effect of pressure on the crater

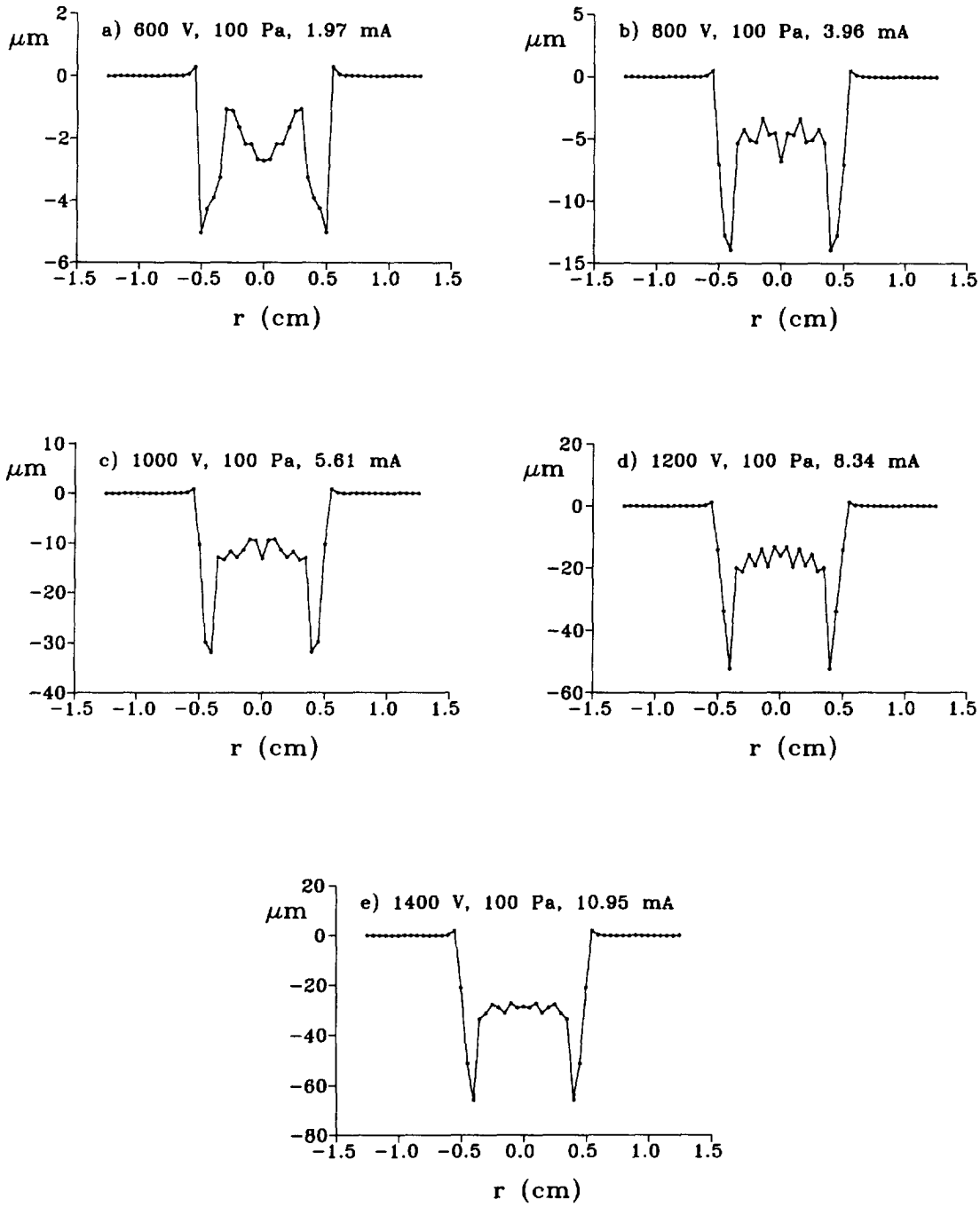

Fig. 9. Calculated crater profiles on the cathode surface after sputtering for 1 h at constant pressure (100 Pa) for five different voltages (and currents) (copper cathode in argon).

profiles after 1 h of sputtering at constant voltage is presented in Fig. 10. Again, the depth of the crater profile increases considerably with pressure, since the current also increases, yielding a larger flux of bombarding particles on the cathode and hence more sputtering. Moreover, the shape of the profile is clearly influenced by the pressure. At 50 Pa, the crater profile is characterized by a pronounced convex shape. As the pressure increases, the convexity decreases, and at 100 Pa a flat crater bottom is attained.

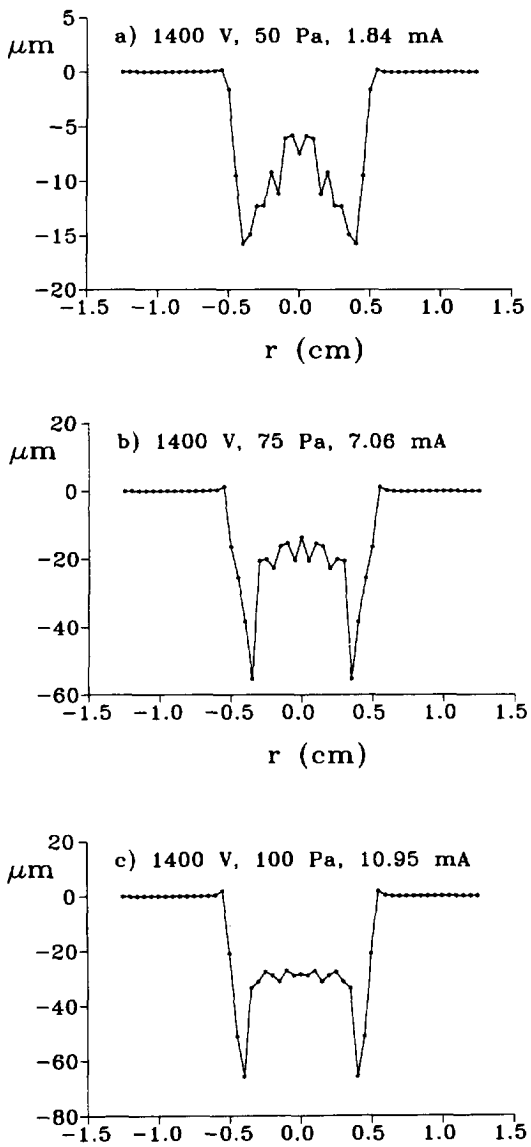

Fig. 10. Calculated crater profiles on the cathode surface after sputtering for 1 h at constant voltage (1400 V) for three different pressures (and currents) (copper cathode in argon).

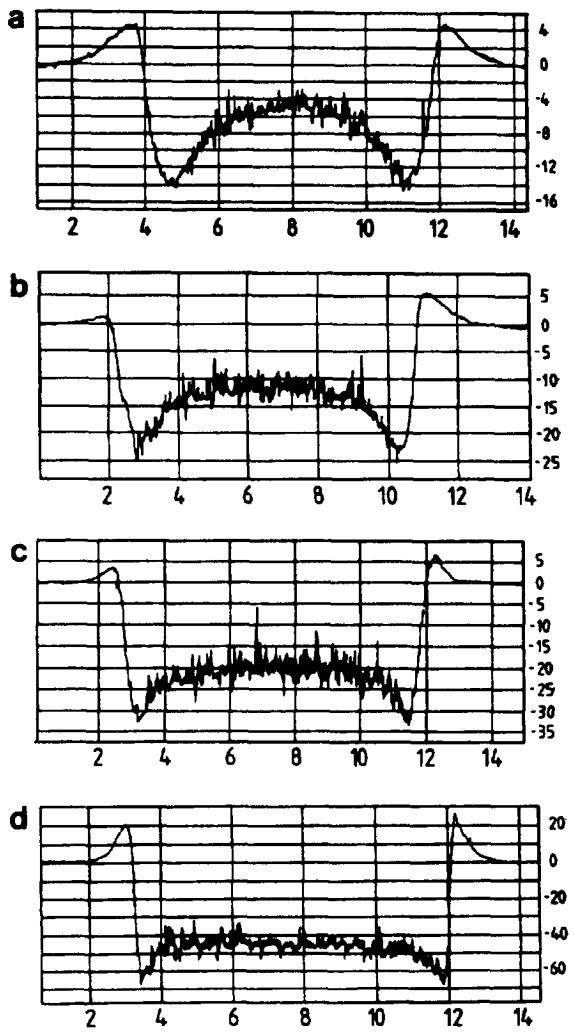

Fig. 11. Experimental crater profiles on the cathode surface after sputtering for 1 h at constant voltage (1000 V) for four different currents (and pressures), obtained with the VG9000 mass spectrometer (copper cathode in argon); (a) 1 mA, (b) 2 mA, (c) 3.5 mA, (d) 6 mA (the x-axis is in mm and the y-axis is in μm) [8].

Hence, the model predicts that it is advisable to work at high pressures, high currents and high voltages to achieve a flat crater bottom. This is in good agreement with experiment. Indeed, Jonkers [8] investigated the influence of voltage and current on the experimental crater profiles in the VG9000 glow discharge cell for analyzing flat samples (the

same cell as used for our modeling work). It was found that by increasing the current at constant voltage (so that the pressure increases) the craters become deeper and the profiles change from a convex character to a more or less flat crater bottom (see Fig. 11 [8]), which is in good agreement with the effects illustrated in Fig. 10. Moreover, by increasing the voltage at constant current, the crater profile changes from a concave to a convex shape (see Fig. 12 [8]). This is also in reasonable agreement with our modeling results. However, the influence of voltage cannot be completely compared, as in the modeling work (Fig. 9) the voltage was increased at constant pressure (so that the current increased too),

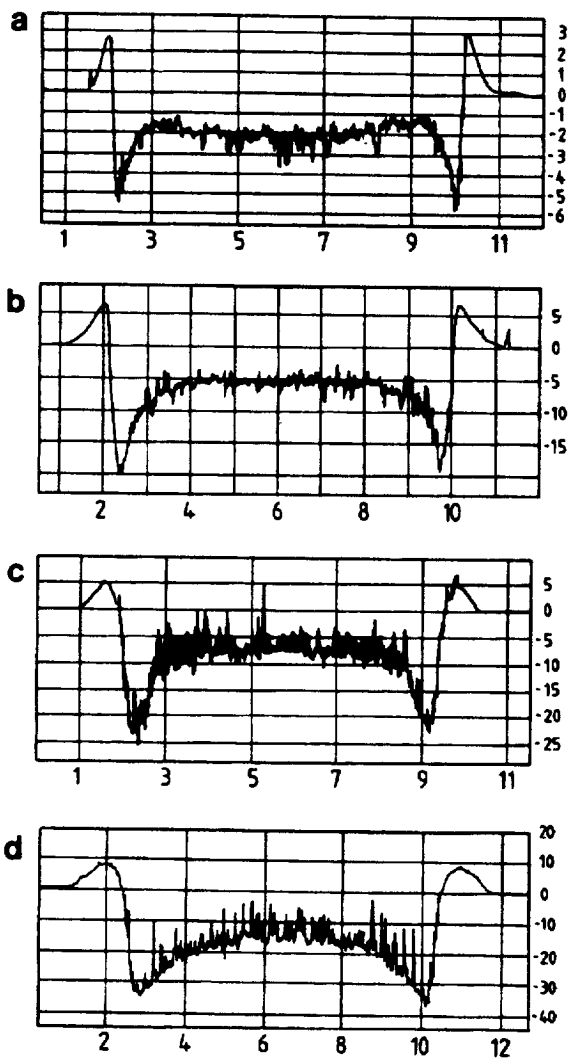

Fig. 12. Experimental crater profiles at the cathode after sputtering for 45 min at constant current (3 mA) for four different voltages (and pressures), obtained with the VG9000 mass spectrometer (copper cathode in argon); (a) 500 V, (b) 750 V, (c) 1000 V, (d) 1250 V (the x-axis is in mm and the y-axis is in μm) [8].

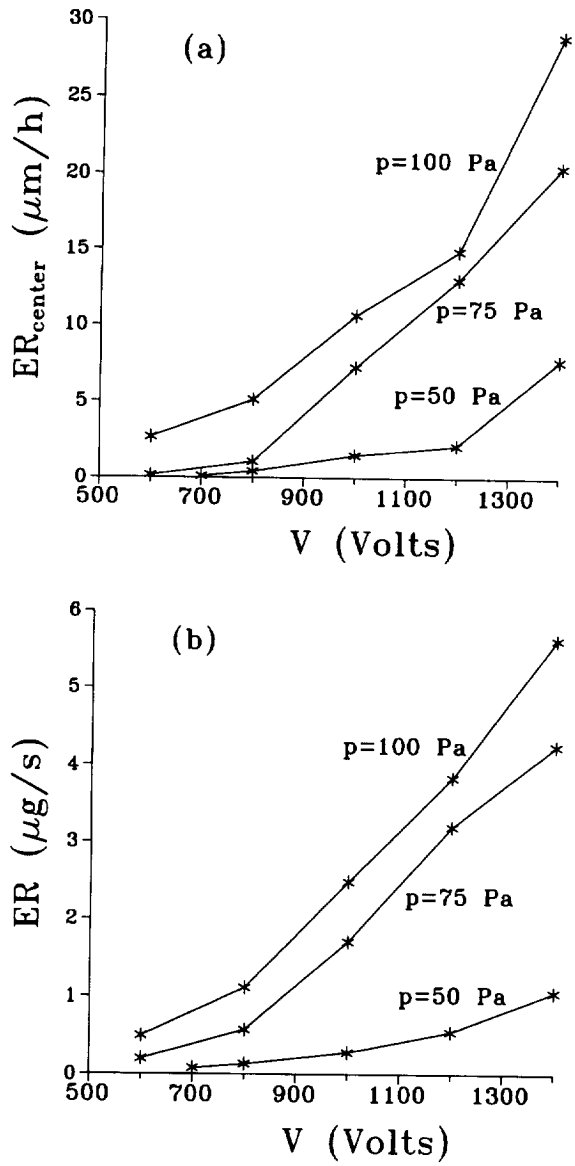

Fig. 13. Calculated erosion rates: (a) in depth per unit time; and (b) in weight loss per unit time, as a function of voltage, at three pressures (copper cathode in argon).

whereas in the experiments of Jonkers, the voltage was increased at constant current (so that the pressure had to decrease). Nevertheless, comparison of Fig. 9(a) and 10(a) indicates that the modeling work also predicts a change from a concave to a convex profile when the voltage increases, the pressure decreases and the current remains more or less constant.

The influence of voltage and pressure on the erosion rate (or in other words on the crater depth at the center of the crater) is presented in Fig. 13(a). The erosion rate rises clearly with voltage and with pressure. Indeed, at higher pressures and voltages, the amount of sputtering increases, since there will be a higher flux of bombarding particles at the cathode and their energies, too, will be higher. The erosion rate increased from 0.1 μm h^{-1} at the lowest pressure and voltage to about 30 μm h^{-1} at the highest pressure and voltage investigated. This is of the same order of magnitude as experimental findings for the VG9000 mass spectrometer [8].

The erosion rate can also be expressed as weight loss per unit time. It can be calculated from the total net flux of sputtered copper atoms by

$$ER = J_{\text{sput, net}} \frac{M}{N_A}$$

where ER is now the erosion rate in g s^{-1}, $J_{\text{sput,net}}$ is the total net sputtered flux (in s^{-1}), and M and N_A are defined above. Fig. 13(b) presents the calculated erosion rates in weight loss as a function of pressure and voltage. It is seen that the erosion rate ranges from 0.1 to 5.6 μg s^{-1}, increasing with voltage and pressure. These values are in reasonable agreement with the typical numbers reported in the literature (e.g., 0.1–10 μg s^{-1} [28], 0.4–1.7 μg s^{-1} [29], 0.8–8 μg s^{-1} [30]).

Although high pressures, voltages and currents seem to yield flatter crater bottoms, and are therefore more useful for depth-profiling, the crater edge effect has not disappeared, i.e. the crater is still deeper at the edges than in the center. This is caused by the front plate at anode potential, which is situated at 0.5 mm from the cathode sample. A similar effect is observed for a Grimm-type glow discharge, where the anode body also approaches the cathode surface very closely [4,31]. Indeed, under all discharge conditions investigated (600–1400 V, 50–100 Pa, 0.5–10 mA), the CDS is calculated to be clearly longer than 0.5 mm (i.e. typically 1.5–5 mm [19,25]), and the equipotential surfaces in the CDS are always found to be slightly bent as in Fig. 4, yielding higher fluxes and energies of bombarding plasma particles at the edges of the crater. It is expected that the crater edge effect cannot be completely eliminated by changing only the discharge conditions; some more fundamental alterations (e.g. in the cell geometry) have to be carried out.

A first possibility is to insert more (or thicker) spacers between cathode and anode front plate, so that these become more separated. Indeed, when the anode front plate is situated near the end of the CDS (for its length, see above), the equipotential surfaces become parallel with the cathode surface, so that there is no focussing of bombarding plasma particles to the edges of the crater, and the electric field near the front plate is no higher than at the cell axis, so that the energies of the bombarding particles are more or less constant as a function of radial position. The usefulness of this method was reported in ref. [31] for a Grimm-type glow discharge. However, when the distance between cathode surface and anode front plate becomes comparable with the length of the CDS, a secondary glow discharge can be created behind the front plate. We do not know the consequences of this phenomenon, whether it disturbs the rest of the discharge or whether it has no influence at all. At least it is expected that the cathode burning spot will become larger. Moreover, the length of the CDS increases considerably with decreasing pressure and slightly with decreasing voltage [19,25]. Hence, when changing discharge conditions, the position of the front plate should be adjusted to be near the end of the CDS by adding or removing spacers, or one should always work with similar discharge conditions. Alternatively, by modifying the shape of the anode front plate (e.g., by cutting the edges), the equipotential surfaces near the front plate will become more nearly parallel to the cathode surface and a flatter crater bottom can be obtained, as was demonstrated in ref. [31] for a Grimm-type glow discharge with a conically (45°) chamfered anode.

Another possible solution to the crater edge effect is to place a mask in front of the cathode sample, with an aperture smaller than the front plate aperture (in the present case, about 4 mm diameter, for example). The mask must also form part of the cathode, so that it will not disturb the electric field distribution in front

of the cathode. The anode front plate still yields higher fluxes and energies of the bombarding plasma particles at the sides of the cathode owing to the non-parallel equipotential surfaces and the higher electric field strengths near the front plate, respectively, but as a mask has been placed in front of the sample the highest amount of sputtering is found at the mask, and the sample is characterized by a flat crater bottom. It is anticipated that a mask constructed of a material with low sputtering yield is desirable, since this yields low sputtering and hence minimal spectral interferences, and also low redeposition on the sample. Tantalum therefore seems to be a good choice. The thickness of the mask is also an important factor: it must be as thin as possible in order to avoid disturbance of the electric potential distribution in front of the cathode, but it should not be too thin or it will immediately be sputtered away. Moreover, the minimum thickness is limited by mechanical (e.g. constructional) considerations. Schelles et al. have evaluated the effect of the thickness of a mask used as secondary cathode for the analysis of nonconductors with the VG9000 mass spectrometer [32]. Although these results apply to nonconductors and cannot be completely adopted here, it is clear that a thin mask (e.g. 0.1 mm) is favorable for minimizing electrical potential disturbances. In refs. [8,10], it was reported that a tantalum mask indeed significantly reduces the crater edge effect. Moreover, the crater side walls become steeper, and there is no deposition of material outside the crater, since the back-diffusing sputtered atoms are redeposited on the mask [8].

Finally, a third possibility would be to completely remove the anode frontplate and to work in a different cell. Some alternative geometries would be the planar diode (i.e. two parallel electrodes placed in a discharge tube made, for example, of glass), or the coaxial cathode (i.e. a direct insertion probe for a flat cathode, in a cell housing serving as anode). It is expected that these cell geometries will be characterized by equipotential surfaces parallel to the cathode surface, and therefore should not suffer from focussing of bombarding plasma particles at some parts of the cathode. In future work, we plan to apply our three-dimensional hybrid models to other cell geometries, to calculate, among other things, the potential distribution explicitly, and to investigate its effect on the crater profiles.

4. Conclusion

The crater profiles at the cathode calculated by our three-dimensional modeling work are in reasonable agreement with experimental results. The calculated profiles for the cell shown in Fig. 1 are not ideal for depth-profiling since they are deeper at the edges than in the center (the so-called "crater edge effect"), have non-steep crater walls, are characterized by a crater rim, and do not always have a flat bottom. The crater edge effect is most pronounced, and is attributed to the anode front plate at 0.5 mm from the cathode surface. Three possible solutions to this problem are proposed: (i) the insertion of more (or thicker) spacers between cathode surface and anode front plate, (ii) the use of a mask in front of the cathode, and (iii) the removal of the anode front plate and operation in a different cell geometry. The first and second possibilities have already been demonstrated to be useful, and the effects of the third solution will be investigated in the near future.

Acknowledgements

A. Bogaerts is indebted to the Belgian National Fund for Scientific Research for financial support. The authors also acknowledge financial support from the Federal Services for Scientific, Technical and Cultural Affairs (DWTC/SSTC) of the Prime Minister's Office through IUAP-III (Conv. 49). Finally, they thank C. Jonkers and P. Van Espen for providing the experimental crater profiles.

References

[1] B. Chapman, Glow Discharge Processes, Wiley, New York, 1980.
[2] R.K. Marcus, Glow Discharge Spectroscopies, Plenum Press, New York, 1993.
[3] H. Hocquaux, Thin Film Analysis, in R.K. Marcus (Ed.), Glow Discharge Spectroscopies, Plenum Press, New York, 1993, Chapter 8.
[4] Z. Weiss, Spectrochim. Acta Part B, 47 (1992) 859.
[5] A. Bengtson, Spectrochim. Acta Part B, 49 (1994) 411.
[6] S. Oswald, V. Hoffmann and G. Ehrlich, Spectrochim. Acta Part B, 49 (1994) 1123.
[7] R. Payling, D.G. Jones and S.A. Gower, Surf. Interface Anal., 23 (1995) 1.

[8] C. Jonkers, Ph.D. Dissertation, University of Antwerp, 1995.
[9] N. Jakubowski and D. Stüwer, J. Anal. At. Spectrom., 7 (1992) 951.
[10] A. Raith, R.C. Hutton and J.C. Huneke, J. Anal. At. Spectrom., 8 (1993) 867.
[11] U. Behn, F.A. Gerbig and H. Albrecht, Fresenius' J. Anal. Chem., 349 (1994) 209.
[12] E. Stumpe, H. Oechsner and H. Schoof, Appl. Phys., 20 (1979) 55.
[13] N. Jakubowski, Ph.D. Dissertation, University of Hohenheim, 1991.
[14] SIMION, Software Version 4.0, Idaho National Engineering Laboratory, Idaho Falls, ID, USA.
[15] A. Bogaerts, R. Gijbels and W.J. Goedheer, Anal. Chem., 68 (1996) 2296.
[16] A. Bogaerts and R. Gijbels, Anal. Chem., 68 (1996) 2676.
[17] A. Bogaerts, M. van Straaten and R. Gijbels, Spectrochim. Acta Part B, 50 (1995) 179.
[18] A. Bogaerts, R. Gijbels and W.J. Goedheer, J. Appl. Phys., 78 (1995) 2233.
[19] A. Bogaerts and R. Gijbels, J. Appl. Phys., 78 (1995) 6427.
[20] A. Bogaerts and R. Gijbels, Phys. Rev. A, 52 (1995) 3743.
[21] N. Matsunami, Y. Yamamura, Y. Itikawa, N. Itoh, Y. Kazumata, S. Miyagawa, K. Morita, R. Shimizu and H. Tawara, At. Data Nucl. Data Tables, 31 (1984) 1.
[22] A. Bogaerts, M. van Straaten and R. Gijbels, J. Appl. Phys., 77 (1995) 1868.
[23] A. Bogaerts and R. Gijbels, J. Appl. Phys., 79 (1996) 1279.
[24] A. Bogaerts and R. Gijbels, Fresenius' J. Anal. Chem., 355 (1996) 853.
[25] A. Bogaerts, Ph.D. Dissertation, University of Antwerp, 1996.
[26] M. van Straaten, R. Gijbels and A. Vertes, Anal. Chem., 64 (1992) 1855.
[27] R.C. Weast and M.J. Astle, CRC Handbook of Chemistry and Physics, 63rd edn., CRC Press, Boca Raton, FL, 1982–1983.
[28] W.W. Harrison, K.R. Hess, R.K. Marcus and F.L. King, Anal. Chem., 58 (1986) 341A.
[29] W.W. Harrison, J. Anal. At. Spectrom., 3 (1988) 867.
[30] K.R. Hess and R.K. Marcus, Spectroscopy, 2 (1987).
[31] D. Demény, L. Szücs and M. Adamik, J. Anal. At. Spectrom., 7 (707) 1992.
[32] W. Schelles, S. Degendt and R. Van Grieken, J. Anal. At. Spectrom., 11 (1996) 937.